C-Reactive Protein Causes Insulin Resistance in Mice Through Fcγ Receptor IIB–Mediated Inhibition of Skeletal Muscle Glucose Delivery

Keiji Tanigaki,[1] Wanpen Vongpatanasin,[2] Jose A. Barrera,[1] Dmitriy N. Atochin,[3] Paul L. Huang,[3] Ezio Bonvini,[4] Philip W. Shaul,[1] and Chieko Mineo[1]

Elevations in C-reactive protein (CRP) are associated with an increased risk of insulin resistance. Whether CRP plays a causal role is unknown. Here we show that CRP transgenic mice and wild-type mice administered recombinant CRP are insulin resistant. Mice lacking the inhibitory Fcγ receptor IIB (FcγRIIB) are protected from CRP-induced insulin resistance, and immunohistochemistry reveals that FcγRIIB is expressed in skeletal muscle microvascular endothelium and is absent in skeletal muscle myocytes, adipocytes, and hepatocytes. The primary mechanism in glucose homeostasis disrupted by CRP is skeletal muscle glucose delivery, and CRP attenuates insulin-induced skeletal muscle blood flow. CRP does not impair skeletal muscle glucose delivery in FcγRIIB$^{-/-}$ mice or in endothelial nitric oxide synthase knock-in mice with phosphomimetic modification of Ser1176, which is normally phosphorylated by insulin signaling to stimulate nitric oxide–mediated skeletal muscle blood flow and glucose delivery and is dephosphorylated by CRP/FcγRIIB. Thus, CRP causes insulin resistance in mice through FcγRIIB-mediated inhibition of skeletal muscle glucose delivery. ***Diabetes*** **62:721–731, 2013**

Numerous clinical studies indicate that chronic, mild increases in circulating levels of the acute-phase reactant C-reactive protein (CRP) are associated with insulin resistance (1–5). For example, in middle-aged men, independent of numerous risk factors including baseline BMI, individuals in the top quintile of CRP (>4.18 μg/mL) had a more than threefold greater risk of developing diabetes than those in the lowest quintile (<0.66 μg/mL) (6). However, the relationship between CRP and type 2 diabetes has been greatly debated (7–10), and whether CRP plays a pathogenetic role is unknown.

In the current study, we determined how CRP influences glucose homeostasis in vivo, testing the hypothesis that CRP induces insulin resistance in mice. Additional studies were performed to address the following questions:

- Which regulatory processes in glucose homeostasis are altered by CRP?
- Is the effect of CRP on glucose homeostasis mediated by Fcγ receptors (FcγR) for IgG, which bind CRP to invoke its cellular actions in certain paradigms (11,12)?
- How does CRP action via FcγR cause insulin resistance?

RESEARCH DESIGN AND METHODS

Animal model. Experiments were performed in male wild-type and CRP-transgenic mice (TG-CRP) on CF-1 or C57BL/6 background (13–16), in endothelial nitric oxide synthase (eNOS)-S1176D knock-in mice (formerly referred to as eNOS-S1179D mice) (17,18), and in FcγRIIB$^{+/+}$, FcγRIIB$^{+/+}$;TG-CRP, FcγRIIB$^{-/-}$, and FcγRIIB$^{-/-}$;TG-CRP littermates (C57BL/6 background) (19). The transgene in the TG-CRP mouse consists of the protein-coding region of the CRP gene linked to the promoter/regulatory region of phosphoenolpyruvate carboxykinase (PEPCK). Although CRP expression can be enhanced by providing these mice a carbohydrate-free diet, such a diet is not necessary for the transgene to be expressed, and the mice fed normal chow display elevated CRP levels (13–16). After weaning, all mice were fed normal chow (Taklad Global 18% Protein Rodent Diet 2018). In select studies, enzyme-linked immunosorbent assays (ELISAs) were used to measure plasma CRP levels (13,14), and levels of tumor necrosis factor-α (TNF-α), adiponectin, and leptin (R&D System or Millipore). The care and use of all study animals was approved by the University of Texas Southwestern Institutional Animal Care and Use Committee and conducted in accordance with Public Health Service Policy on the Humane Care and Use of Laboratory Animals.

Glucose (GTT) and insulin tolerance tests (ITT). Mice were fasted for 4–6 h and injected intraperitoneally with D-glucose (1 g/kg body weight) for GTT or with insulin (1 units/kg body weight) for ITT. Tail vein blood samples were obtained at the indicated times for plasma glucose measurement by glucometer (ONE TOUCH Ultra2, Johnson & Johnson). Plasma insulin concentrations were determined by ELISA (Crystal Chem Inc.).

Glucose infusion rate (GIR). After a 5-h fast, euglycemic-hyperinsulinemic clamps were performed with an insulin infusion at 20 mU/kg/min for 180 min. Euglycemia (1.20–1.40 g/L) was maintained by measuring blood glucose every 10 min and adjusting a variable infusion of glucose. GIR was calculated as the mean of the values administered in 10-min intervals during the 180-min infusion period (20,21).

Administration of CRP. Mice were intraperitoneally injected with human recombinant CRP (200 μg, Calbiochem) or an equal volume of vehicle (140 mmol/L NaCl, 20 mmol/L Tris-HCl, 2 mmol/L $CaCl_2$, 0.05% NaN_3, pH 7.5) every other day for 14 days. This dose was chosen based on initial pharmacokinetic studies indicating a CRP serum half-life of 5.3 h and that an intraperitoneal dose of 200 μg yielded an average serum CRP of 31 μg/mL over the ensuing 48 h.

In vivo and ex vivo glucose uptake. In vivo glucose uptake was measured as previously reported (22). Briefly, fasted mice were injected intraperitoneally with 2-deoxy-[^{3}H]glucose ([^{3}H]-2-DOG, Amersham; 2 g/kg; 10 μCi/mouse) mixed with dextrose (20%), and blood glucose was measured at 0–90 min. The plasma was deproteinized with ice-cold perchloric acid (3.5%), the supernatant was neutralized with 2.2 mol/L $KHCO_3$, and radioactivity was determined in a liquid scintillation counter. The glucose-specific activity (degenerations/min/μmol) was calculated by dividing the radioactivity by the glucose concentration, and the area under the curve (AUC) was integrated for the duration of the experiment (90 min). Skeletal muscle (soleus and gastrocnemius) and

From the [1]Division of Pulmonary and Vascular Biology, Department of Pediatrics, University of Texas Southwestern Medical Center, Dallas, Texas; the [2]Hypertension Section, Cardiology Division, Department of Internal Medicine, University of Texas Southwestern Medical Center, Dallas, Texas; the [3]Cardiovascular Research Center and Cardiology Division, Department of Medicine, Massachusetts General Hospital and Harvard Medical School, Boston, Massachusetts; and [4]MacroGenics, Inc., Rockville, Maryland.
Corresponding author: Chieko Mineo, chieko.mineo@utsouthwestern.edu.
Received 9 February 2012 and accepted 17 August 2012.
DOI: 10.2337/db12-0133
This article contains Supplementary Data online at http://diabetes.diabetesjournals.org/lookup/suppl/doi:10.2337/db12-0133/-/DC1.

See accompanying commentary, p. 688.

perigonadal white adipose tissue were harvested at 90 min. Peak plasma insulin concentrations during the in vivo glucose uptake experiments were 0.25 ± 0.03 nmol/L and 0.35 ± 0.04 nmol/L for wild-type and TG-CRP mice, respectively (13-week-old males, $n = 6$; P = NS).

To measure tissue accumulation of 2-deoxy-[^{3}H]2DOG-6-phosphate ([^{3}H]2-DOG-6-phosphate), the harvested tissues were homogenized, and the homogenate was precipitated in ice-cold perchloric acid (7%). After the centrifugation, the supernatant was neutralized for 30 min with 2.2 mol/L $KHCO_3$, and two aliquots were prepared. One aliquot was used to determine total ^{3}H radioactivity. The other aliquot was passed through an anion exchange column (AG 1-X8 resin; Bio-Rad Laboratories) to remove unbound [^{3}H]2-DOG-6-phosphate. The column was washed with distilled water, and the radioactivity in the eluted volume was measured in a scintillation counter. The difference between total and eluted ^{3}H radioactivity represents accumulated [^{3}H]2-DOG-6-phosphate. The protein pellet was digested with 1N KOH, and protein concentration was determined by Bradford assay (Bio-Rad Laboratories). To calculate [^{3}H]2-DOG uptake, the radioactive counts (degenerations/min) were divided by the integrated glucose-specific activity AUC and the sample protein content.

In ex vivo studies, basal and insulin-stimulated glucose uptake in soleus and extensor digitorum longus muscle was measured as previously described (23). Briefly, the muscles were excised and incubated at 30°C in the absence or presence of 2 nmol/L insulin for 40 min in Krebs-Henseleit buffer supplemented with 5 mmol/L Hepes, 0.1% BSA, and 2 mmol/L pyruvate. Muscles were further incubated for an additional 20 min in Krebs-Henseleit buffer containing 1 mmol/L [^{3}H]2-DOG (2.5 mCi/mL) and 19 mmol/L [^{14}C]mannitol (0.7 mCi/mL) at 30°C. After incubation, muscles were digested in 0.5 mol/L NaOH, and extracellular space and intracellular 2-deoxyglucose concentrations were determined. Glucose uptake experiments were also performed as previously described using 3T3L1 cells that were differentiated into adipocytes (24).

Insulin-induced skeletal muscle blood flow. After a 5-h fast, mice were anesthetized with isoflurane, and the left carotid artery was cannulated for measurement of blood pressure and the right jugular vein for infusion of glucose and insulin. The right femoral artery was exposed via a 1.5-cm incision and separated from the femoral vein and nerve. The epigastric branch, which provides blood flow to the skin and adipose tissue but not to skeletal muscle, was ligated. A 0.3-mm flow probe was positioned over the femoral artery to measure blood flow, blood pressure, and heart rate using a pulsed Doppler flow system (Crystal Biotech, Holliston, MA). After a 45–60-min equilibration period, a 180-min euglycemic-hyperinsulinemic clamp (blood glucose 1.20–1.40 g/L) was performed with an insulin infusion at 20 mU/kg/min, and blood flow data were recorded throughout using Powerlab data acquisition software (ADInstruments, Bella Vista, Australia).

Hepatic glucose production. Surgical and experimental procedures are previously described (25). Mice were surgically implanted with an indwelling jugular vein catheter externalized on the nape of the neck and then recovered for 5 days. Mice that lost >10% of presurgical body weight were not studied. On the day of study, mice were transferred to a sterile shoebox-sized cage lined with bedding at 9:00 A.M. to begin a 5-h fast. At t = −120 min, water was removed and a primed, continuous infusion of [3-^{3}H]glucose (5-μCi bolus + 0.05 μCi/min) was initiated. At t = −15 and −5 min, blood samples from the cut tail were taken to measure basal fasted blood glucose, plasma insulin, and glucose turnover. At t = 0 min, a continuous infusion of insulin (Humulin; 4 mU/kg/min) was used to induce hyperinsulinemia. The infusion of [3-^{3}H]glucose was increased to 0.1 μCi/min to account for changes in specific activity. Blood samples were taken every 10 min thereafter to measure blood glucose. A variable GIR (50% dextrose) was used to maintain blood glucose at ~1.50 g/L. Additional blood samples were taken every 10 min during the steady-state period (t = 80–120 min) to determine plasma insulin, endogenous rate of glucose appearance, and rate of glucose disappearance. Endogenous rate of glucose appearance and rate of glucose disappearance were calculated using Steele's non-steady-state Eqs (26,27). Plasma insulin concentrations during the clamp were 0.14 ± 0.05 and 0.15 ± 0.04 nmol/L for wild-type and TG-CRP mice, respectively (n = 4–6; P = NS).

Metabolic and body composition measurements. Indirect calorimetry and locomotion data were simultaneously measured using the Comprehensive Laboratory Animal Monitoring System (Columbus Instruments). Fat mass and lean body mass were determined by NMR (Minispec NMR Analyzer; Bruker).

Quantitative PCR analyses. To evaluate FcγRIIB expression in pancreatic islets, islets were isolated from wild-type CF1 mice (28), and quantitative real-time PCR was performed using an Applied Biosystems 7900HT sequence detection system and SYBR-green chemistry (Applied Biosystems, Foster City, CA) with gene-specific primers (forward 5′-TCCTCCTGATCTGGAAGAAGCT-3′ and reverse 5′-CGGGATGCTTGAGAAGTGAGT-3′).

To evaluate inflammation genes and macrophage markers in adipose tissue, total RNA was extracted and purified from epididymal white adipose tissue, and reverse transcription was performed, followed by real-time quantitative PCR using a Roche LightCycler 480 and iQ SYBR Green Supermix (Bio-Rad). Relative amounts of target products were quantified by comparative C_T method ($\Delta\Delta C_T$), normalized to β-actin. Primer sequences were TNF-α: forward 5′-CATCTTCTCAAAATTCGAGTGACAA-3′ and reverse 5′-TGGGAGTAGACAAGGTACAACCC-3′; interleukin (IL)-6: forward 5′-GAGGATACCACTCCCAACAGACC-3′ and reverse 5′-AAGTGCATCATCGTTGTTCATACA; F4/80: forward CTTTGGCTATGGGCTTCCAGTC-3′ and reverse 5′-GCAAGGAGGACAGAGTTTATCGTG-3′; and Mac-2: forward 5′-ATGAAGAACCTCCGGGAAAT-3′ and reverse 5′-GCTTAGATCATGGCGTGGTT-3′.

Immunohistochemical analyses. Expression of FcγRIIB was evaluated by immunohistochemistry in tissues from FcγRIII$^{-/-}$ mice with a chimeric antibody (ch2.4G N297Q) directed to mouse FcγRIIB and FcγRIII. This antibody is a modified 2.4G antibody in which Asn297 in the Fc domain has been mutated to Gln to prevent Fc-FcR binding, thereby minimizing nonspecific binding. A standard indirect immunoperoxidase horseradish peroxidase method was used to incubate tissue sections with ch2.4G N297Q or an isotype-matched negative control antibody, followed by peroxidase-conjugated secondary goat anti-human (H+L) IgG (Jackson Immunoresearch). Slides were further incubated with 3-amino-9 ethylcarbazole (Vector) and counterstained with Gill's hematoxylin. For immunofluorescence analysis of FcγRIIB in skeletal muscle from FcγRIIB$^{+/+}$ and FcγRIIB$^{-/-}$ mice, tissue sections were incubated with rat anti-mouse CD31 (BD Pharmingen), followed by ch2.4G N297Q Alexa488 conjugated (MacroGenics) or an isotype-matched negative control antibody overnight at 4°C. Slides were incubated with Cy3-conjugated donkey anti-rat IgG (Jackson ImmunoResearch) for 1 h, washed in PBS, and mounted.

Statistical analysis. Comparisons between two groups were performed by Student t tests. Differences between multiple groups were evaluated by one-way ANOVA and Student-Newman-Keuls post hoc testing. Values shown are mean ± SEM. Significance was accepted at the 0.05 level of probability.

RESULTS

CRP causes insulin resistance in mice. We first studied glucose and insulin homeostasis in 14–16-week-old male wild-type controls and TG-CRP mice. Compared with controls, fasting glucose and insulin levels were elevated in TG-CRP mice (Fig. 1*A* and *B*). TG-CRP mice also displayed abnormal GTT (Fig. 1*C*) and ITT (Fig. 1*D*). Plasma CRP levels were undetectable (<1 μg/mL) in controls and were 3–14 μg/mL in TG-CRP mice. Abnormal GTT and ITT were observed across the range of CRP levels studied (data not shown). The GIR was measured during a euglycemic-hyperinsulinemic clamp and was decreased >50% in TG-CRP versus control mice (Fig. 1*E*). Thus, TG-CRP mice with modest increases in CRP at levels known to be associated with the development of type 2 diabetes in humans (1–4,6) have insulin resistance.

We next investigated the age at which TG-CRP mice display abnormal glucose and insulin homeostasis and evaluated the effect of CRP on body weight and composition. Both 5- and 13-week-old male TG-CRP mice displayed fasting hyperglycemia and hyperinsulinemia (Fig. 2*A* and *B*). At 5 weeks, TG-CRP mice had body weights below those of wild-type mice and had a lower percentage of fat mass (Fig. 2*C*–*E*). At 13 weeks, TG-CRP and wild-type mice had similar body weights, but TG-CRP mice had a greater percentage of fat mass. Therefore, TG-CRP mice develop abnormal glucose and insulin homeostasis before an increase in fat mass. Studies in metabolic chambers revealed that TG-CRP mice did not have alterations in oxygen consumption, CO_2 production, respiratory exchange rate, heat production, or food intake compared with wild-type mice (Supplementary Fig. 1*A*–*E*).

Plasma adiponectin levels were 8.69 ± 0.54 and 9.31 ± 0.46 μg/mL (n = 8/group), and leptin levels were 11.35 ± 1.20 and 14.43 ± 2.86 ng/mL (n = 8/group) in wild-type and TG-CRP mice, respectively, indicating that they are not altered by CRP in vivo. Plasma levels of TNF-α were undetectable in controls and in TG-CRP mice. There were also no differences in mRNA abundance for TNF-α or IL-6

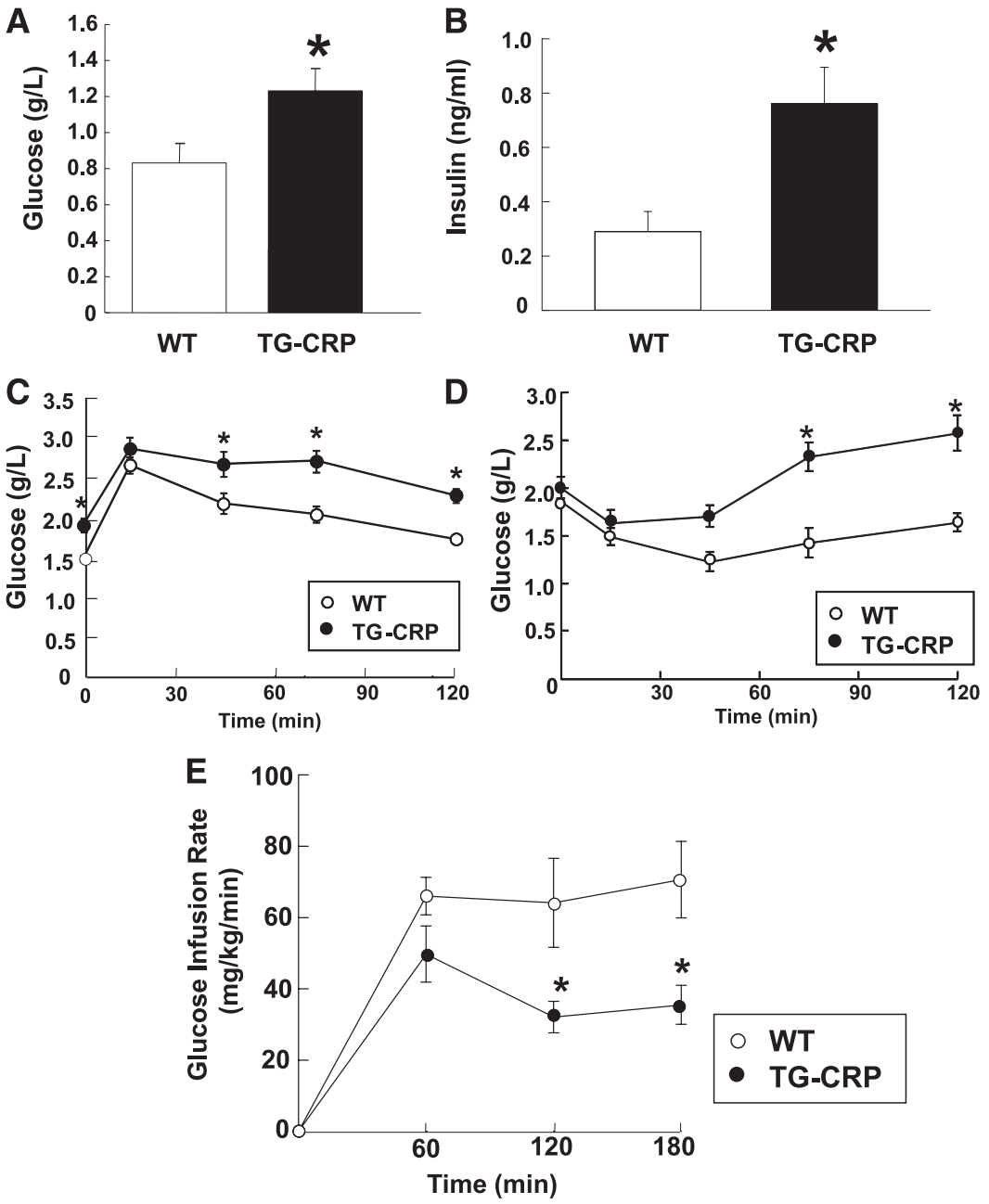

FIG. 1. TG-CRP mice display fasting hyperglycemia, hyperinsulinemia, and insulin resistance. Fasting plasma levels of glucose (*A*) and insulin (*B*) were measured in wild-type (WT) or TG-CRP mice (14–16 weeks old; $n = 10$). Glucose tolerance tests (*C*) and insulin tolerance tests (*D*) were evaluated, as were GIRs during euglycemic-hyperinsulinemic clamps with 20 mU/min/kg insulin (*E*) ($n = 5$–10). Values are mean ± SEM. *$P < 0.05$ vs. wild-type.

or for the macrophage markers F4/80 and Mac-2 in adipose tissue isolated from wild-type versus TG-CRP mice (data not shown). Thus, CRP alone does not cause systemic inflammation or promote inflammation in adipose tissue.

We next determined if the administration of CRP alters glucose and insulin homeostasis in wild-type male mice given recombinant human CRP or vehicle by intraperitoneal injection every other day for 14 days. Whereas vehicle-treated mice showed no changes, CRP-treated mice displayed fasting hyperglycemia and hyperinsulinemia on day 15 of the study (Fig. 3*A* and *B*). Shorter duration of CRP treatment (7 or 11 days) did not alter fasting glucose or insulin (data not shown). Body weight and fat and lean body mass were not affected by CRP treatment (Fig. 3*C*–*E*). These results provide further evidence that CRP causes insulin resistance in vivo and that it does so independently of changes in body composition.

FcγRIIB mediates CRP-induced insulin resistance. The FcγRs are IgG receptors that invoke the cellular actions of CRP in certain paradigms (11,12). To begin to determine how CRP causes insulin resistance, we tested the potential role of the inhibitory FcγR isoform designated FcγRIIB (29) in studies of FcγRIIB$^{+/+}$;TG-CRP, FcγRIIB$^{-/-}$;TG-CRP, FcγRIIB$^{+/+}$, and FcγRIIB$^{-/-}$ littermates. Fasting glucose and insulin levels were elevated in FcγRIIB$^{+/+}$;TG-CRP versus controls (FcγRIIB$^{+/+}$) but were normal in FcγRIIB$^{-/-}$;TG-CRP mice (Fig. 4*A* and *B*). Furthermore, GTT and ITT revealed that whereas FcγRIIB$^{+/+}$;TG-CRP

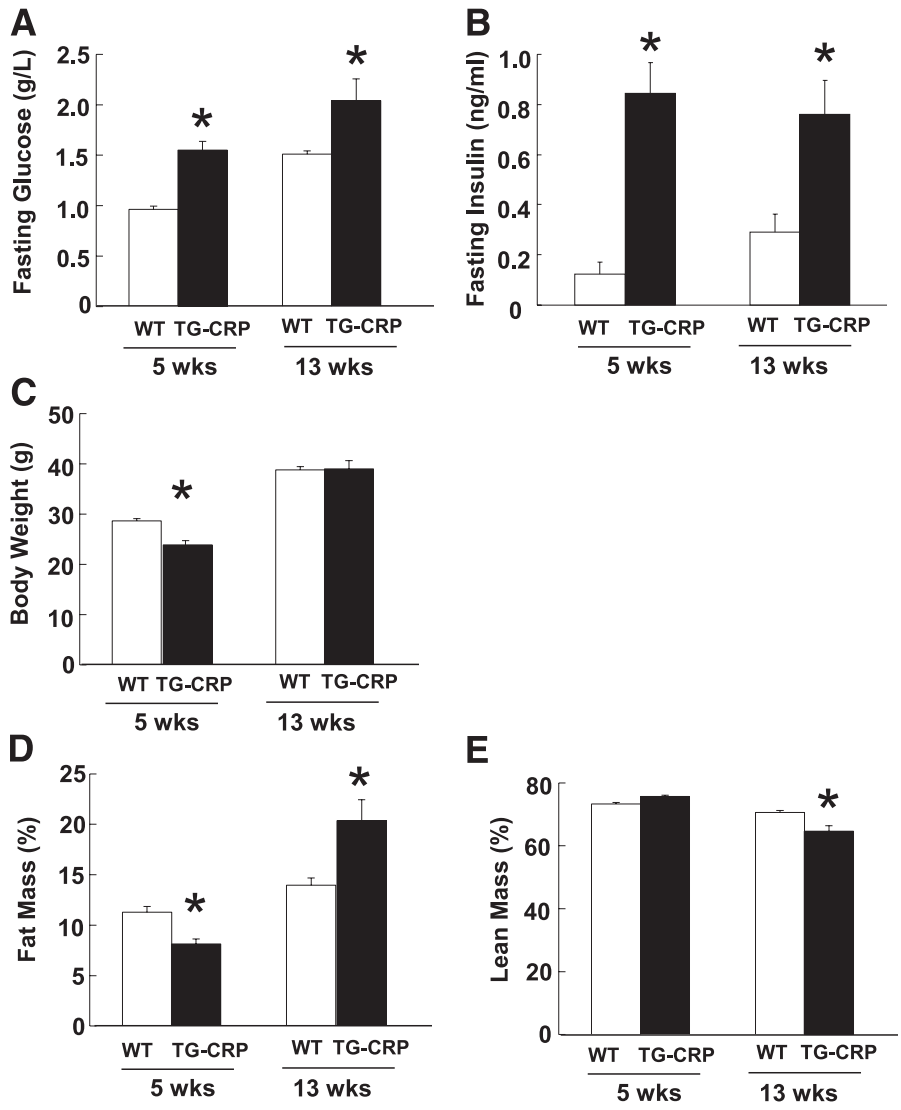

FIG. 2. TG-CRP mice develop insulin resistance at an early age. Fasting plasma levels of glucose (*A*) and insulin (*B*), body weight (*C*), fat mass (*D*), and lean body mass (*E*) were measured in wild-type (WT) and TG-CRP mice at the age of 5 or 13 weeks. Values are mean ± SEM, $n = 6$. *$P < 0.05$ vs. wild-type.

have glucose intolerance and decreased insulin sensitivity, FcγRIIB$^{-/-}$;TG-CRP have normal glucose tolerance and normal insulin sensitivity (Fig. 4*C* and *D*). Thus, FcγRIIB is required for CRP-induced insulin resistance.

We next evaluated FcγRIIB protein distribution in tissues from FcγRIII$^{-/-}$ mice with a chimeric antibody that recognizes both mouse FcγRIIB and FcγRIII. Microvascular endothelium in heart, brain, liver, and kidney displayed signal for FcγRIIB (data not shown). Importantly, positive microvascular endothelial cell staining was abundant in skeletal muscle (gastrocnemius) (Fig. 4*E*). Staining was negative with control unrelated IgG or with ch2.4G N297Q antibody applied to tissues from FcγRIIB$^{-/-}$ mice (Supplementary Fig. 2). In skeletal muscle there was colocalization of the receptor with the endothelial cell marker platelet endothelial cell adhesion molecule-1(Fig. 4*F*), whereas it was not detected in myocytes (Fig. 4*E* and *F*, Supplementary Fig. 2), adipocytes, or hepatocytes (data not shown). Thus, the microvascular endothelium in the skeletal muscle is the well-recognized insulin target cell in which FcγRIIB is expressed.

CRP blunts skeletal muscle glucose delivery. To delineate the basis for the adverse effects of CRP on glucose and insulin homeostasis, we evaluated numerous processes. Wild-type and TG-CRP mice both had elevations in plasma insulin in response to glucose (Fig. 5*A*), indicating comparable capacity for pancreatic insulin secretion. This finding is consistent with a lack of FcγRIIB mRNA expression in pancreatic islets (data not shown). We also measured hepatic glucose production and found that CRP did not alter basal production or the fall in production in response to insulin (Fig. 5*B*).

We next determined if CRP affects tissue glucose delivery in studies of [^{3}H]-2-DOG uptake in perigonadal white adipose tissue and gastrocnemius and soleus in male mice aged 10–13 weeks. Glucose uptake in white adipose was comparable in control and TG-CRP mice (Fig. 5*C*). Consistent with this finding, CRP did not alter glucose uptake in differentiated adipocytes in culture (Supplementary Fig. 3). In contrast, TG-CRP mice displayed 39% less skeletal muscle glucose uptake than wild-type mice (Fig. 5*D*). The selective impact of CRP on

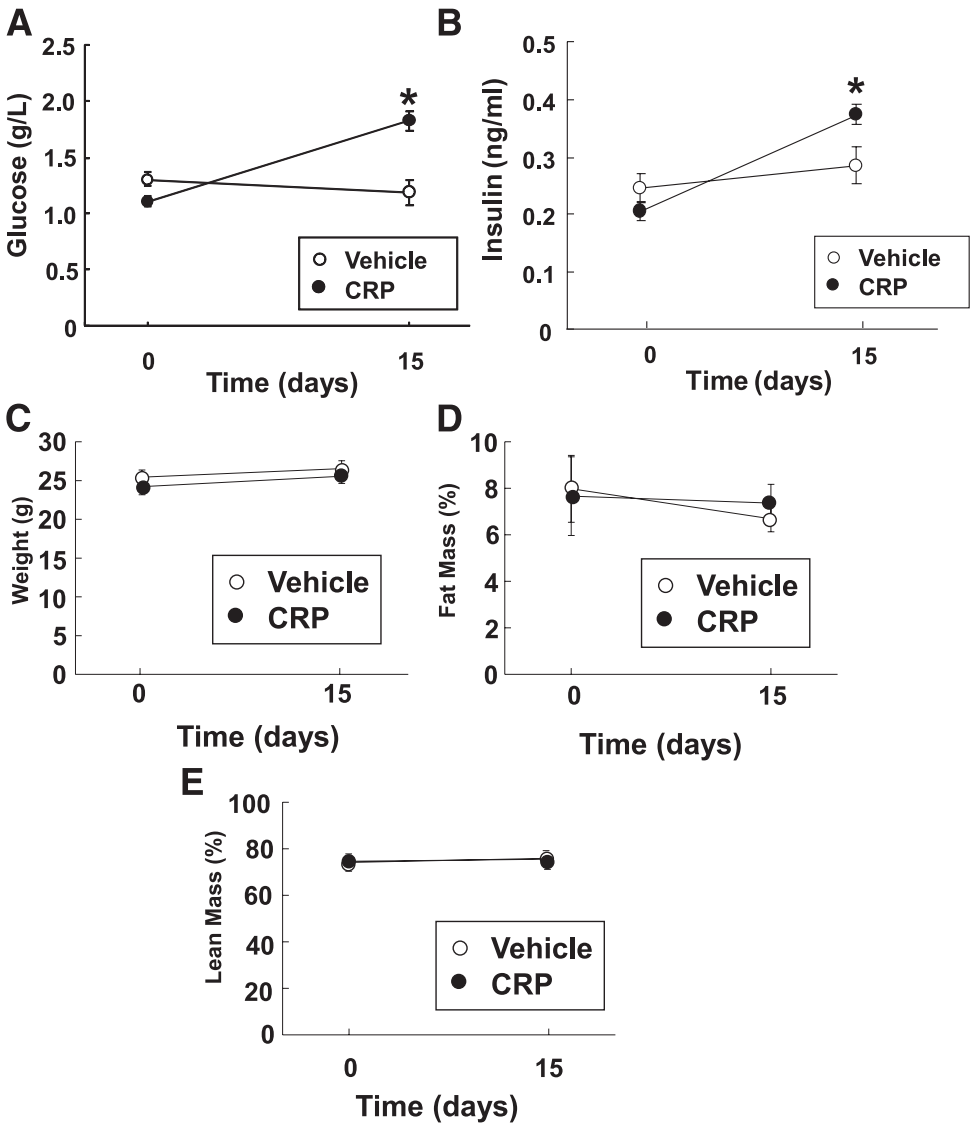

FIG. 3. Exogenous CRP administration causes fasting hyperglycemia and hyperinsulinemia without altering body composition. Wild-type mice were intraperitoneally injected with vehicle or CRP every other day for 14 days. On days 0 and 15, fasting plasma levels of glucose (*A*) and insulin (*B*), body weight (*C*), fat mass (*D*), and lean mass (*E*) were measured. Values are mean ± SEM, n = 7–14. *P < 0.05 vs. vehicle.

skeletal muscle and not adipose glucose delivery was also apparent at age 5–6 weeks (Fig. 5*E* and *F*). Having discovered an abundance of FcγRIIB in skeletal muscle microvascular endothelium (Fig. 4*E* and *F*; Supplementary Fig. 2), in which insulin activates eNOS (30,31) to increase blood flow and microvascular recruitment and thereby promote glucose disposal (32–35), we next studied insulin-induced skeletal muscle blood flow in the hind limb. Basal blood flow was similar in control and TG-CRP mice (0.339 ± 0.152 and 0.234 ± 0.08 cm/s, respectively, n = 5; P = NS). However, whereas insulin infusion increased muscle blood flow by 60% in control mice (Fig. 5*G*), there was a complete lack of response in TG-CRP mice. To then confirm these findings by another means, we studied the effect of CRP treatment in wild-type mice. Whereas CRP administration did not affect glucose delivery to white adipose tissue (Fig. 5*H*), glucose delivery to skeletal muscle was decreased (Fig. 5*I*). Thus, the primary mechanism in glucose homeostasis disrupted by CRP is skeletal muscle glucose delivery, and this is associated with an impaired response of the skeletal muscle vasculature to insulin.

FcγRIIB and eNOS antagonism mediate CRP impairment of muscle glucose delivery. Because FcγRIIB, which is required for CRP-induced insulin resistance (Fig. 4*A–D*), is not expressed in skeletal muscle myocytes (Fig. 4*E* and *F*), the decrease in muscle glucose delivery caused by CRP is unlikely to be due to direct actions on insulin signaling in myocytes. This conclusion was strengthened in ex vivo studies of insulin-induced glucose transport in soleus and extensor digitorum longus muscles (Fig. 6*A* and *B*), which revealed similar insulin responses in muscles from wild-type and TG-CRP mice. To further determine whether the primary impact of CRP on glucose homeostasis occurs through actions on endothelium, changes in in vivo glucose uptake in response to CRP treatment were compared in wild-type versus eNOS-S1176D knock-in mice expressing a phosphomimetic form of eNOS (18). Insulin signaling in endothelial cells normally stimulates the phosphorylation of eNOS-S1176 (murine isoform, S1177 in human,

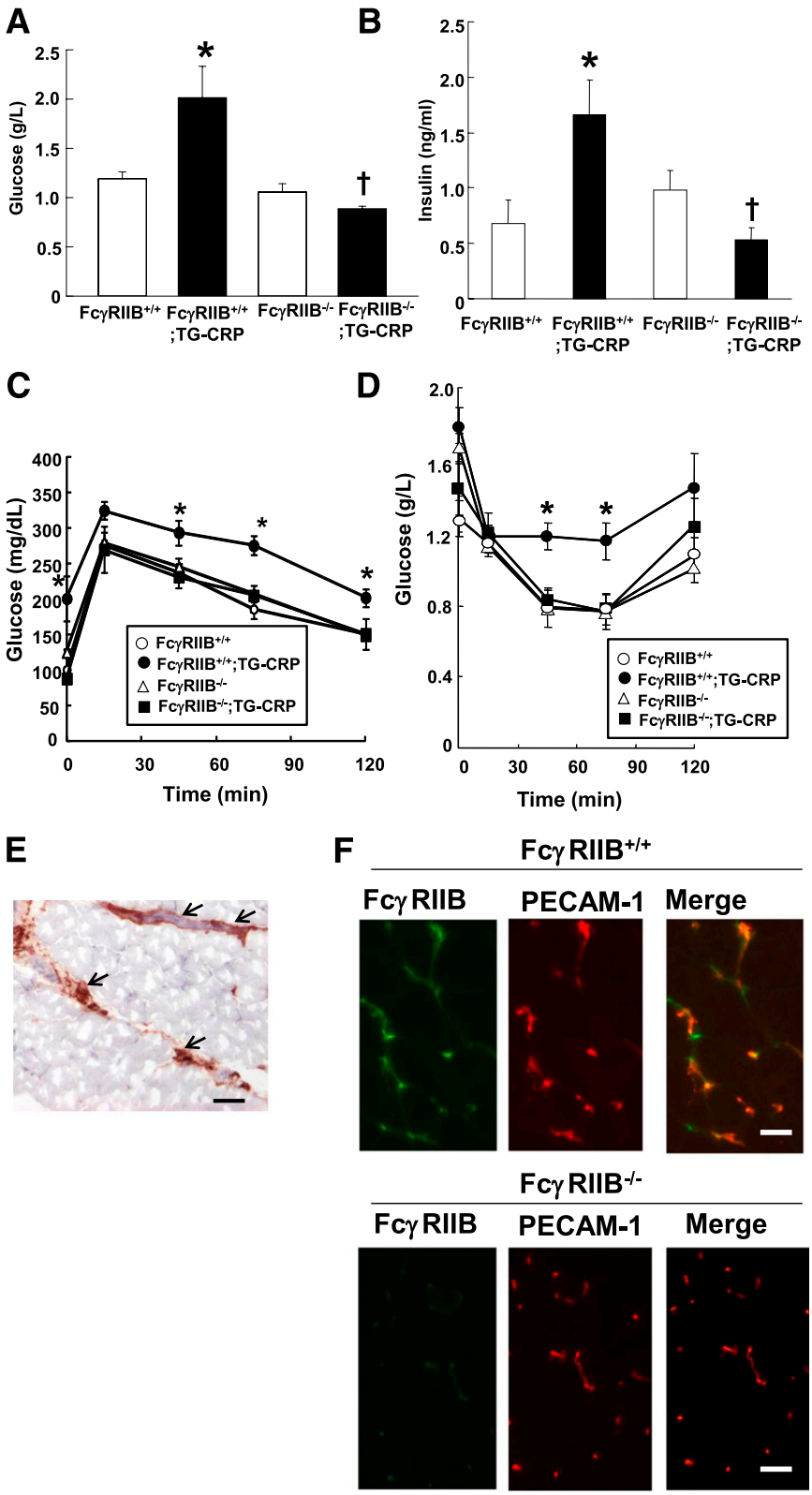

FIG. 4. CRP-induced insulin resistance is mediated by FcγRIIB, which is expressed in skeletal muscle microvascular endothelium. Fasting glucose (*A*) and insulin (*B*) levels were measured in FcγRIIB$^{+/+}$, FcγRIIB$^{+/+}$;TG-CRP, FcγRIIB$^{-/-}$, and FcγRIIB$^{-/-}$;TG-CRP littermates. Values are mean ± SEM, n = 4–8. *P < 0.05 vs. FcγRIIB$^{+/+}$, †P < 0.05 vs. FcγRIIB$^{+/+}$;TG-CRP. Glucose tolerance tests (*C*) and insulin tolerance tests (*D*) were performed in the same groups. Values are mean ± SEM, n = 4–8. *P < 0.05 vs. FcγRIIB$^{+/+}$ at the indicated times. *E*: Expression of FcγRIIB in skeletal muscle. Immunostaining for FcγRIIB was performed on gastrocnemius from FcγRIII$^{-/-}$ mice with chimeric antibody to mouse FcγRIIB and FcγRIII (ch2.4G2, N297Q). Positive signal for FcγRIIB was detected in the microvascular endothelium (arrows) and was absent in skeletal muscle myocytes. Scale bars = 50 μm. *F*: FcγRIIB expression in skeletal muscle was assessed by immunofluorescence in tissue from FcγRIIB$^{+/+}$ vs. FcγRIIB$^{-/-}$ mice. The skeletal muscle sections were probed with anti-FcγRII (green) and anti-platelet endothelial cell adhesion molecule-1 (PECAM-1; red) antibodies. Merged images are also shown. Scale bars = 50 μm. (A high-quality digital representation of this figure is available in the online issue.)

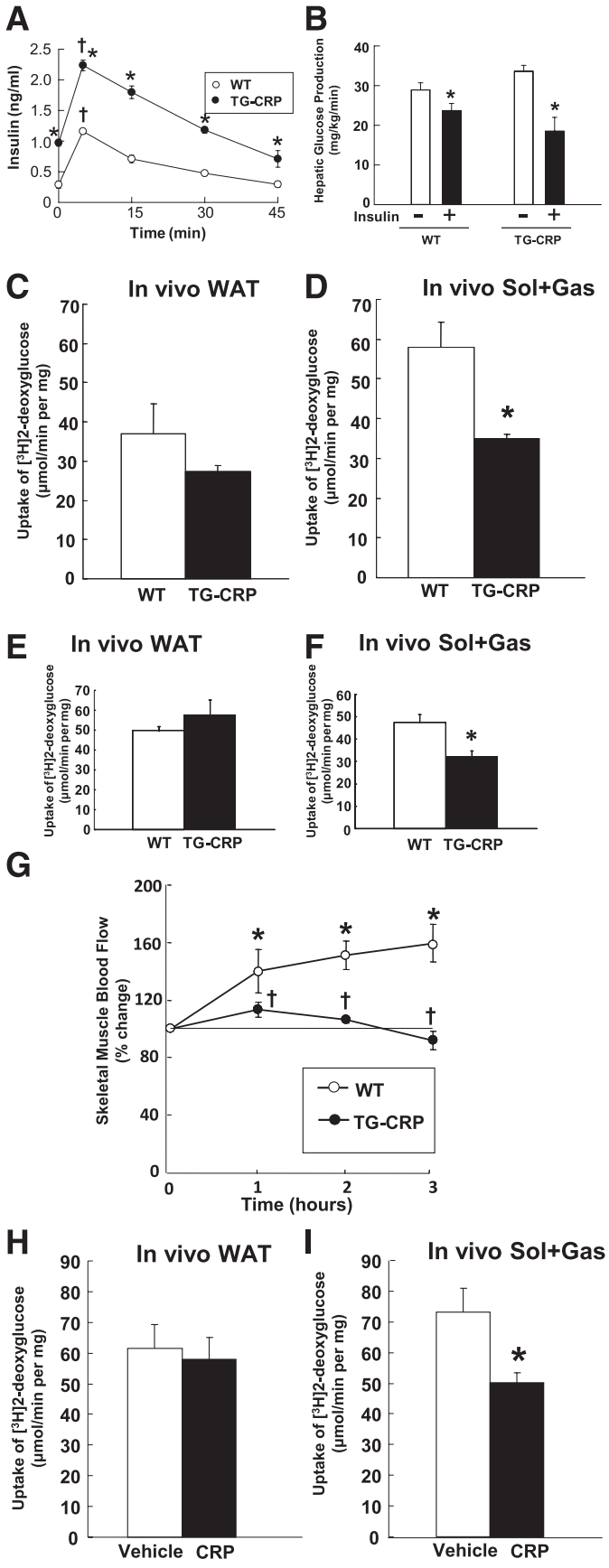

FIG. 5. CRP decreases skeletal muscle glucose delivery and insulin-induced skeletal muscle blood flow and does not alter pancreatic insulin secretion or hepatic glucose production. *A*: Pancreatic insulin secretion was evaluated in 10–13-week-old wild-type (WT) and TG-CRP mice. After an intraperitoneal injection of D-glucose, plasma insulin levels were measured at the indicated times. Values are mean ± SEM, $n = 8$. *$P < 0.05$ vs. wild-type at the indicated time, †$P < 0.05$ vs. time 0. *B*: Hepatic glucose production was measured at baseline and during a hyperinsulinemic-euglycemic

S1179 in bovine) (30,34) to activate the enzyme and increase muscle blood flow and microvascular recruitment and thereby promote glucose disposal (33–35). In prior work we showed that the CRP/FcγRIIB tandem inhibits eNOS activation by causing eNOS-S1176 dephosphorylation (36,37). Therefore, the phosphomimetic eNOS in eNOS-S1176D mice is resistant to CRP antagonism (18,36,37). CRP did not alter glucose uptake in white adipose tissue of wild-type or eNOS-S1176D mice (Fig. 6*C*). However, whereas CRP blunted glucose uptake in the skeletal muscle of wild-type mice, as previously observed (Fig. 5*D*), uptake was unaffected by CRP in eNOS-S1176D mice (Fig. 6*D*).

Now knowing that eNOS antagonism by CRP underlies the impairment in muscle glucose disposal, and knowing that FcγRIIB mediates CRP inhibition of eNOS (36,37), it would be predicted that FcγRIIB is required for CRP to blunt muscle glucose delivery. Additional glucose uptake experiments were therefore performed in FcγRIIB$^{+/+}$;TG-CRP, FcγRIIB$^{-/-}$;TG-CRP, FcγRIIB$^{+/+}$, and FcγRIIB$^{-/-}$ littermates. Glucose uptake in white adipose tissue was comparable in the four groups (Fig. 6*E*), and as expected, muscle glucose uptake was impaired in FcγRIIB$^{+/+}$;TG-CRP versus FcγRIIB$^{+/+}$ mice (Fig. 6*F*). In contrast, muscle glucose uptake was not adversely affected by CRP in FcγRIIB$^{-/-}$;TG-CRP mice. These cumulative findings indicate that CRP impairs skeletal muscle glucose delivery, that this is caused by CRP attenuation of the endothelial actions of insulin in skeletal muscle, and that FcγRIIB in the muscle microvasculature mediates this process.

DISCUSSION

Numerous studies have indicated that chronic, modest elevations in CRP are associated with the development of insulin resistance in humans (1–6). However, there has been debate whether these associations are independent of the relative degree of adiposity of the individual or an epiphenomenon of obesity (7–10). Furthermore, it has been unknown whether CRP is a pathogenetic factor in insulin resistance. We therefore investigated the direct effects of CRP on insulin sensitivity in mice and discovered, using multiple strategies, that modest elevations in CRP cause insulin resistance. These findings reveal an entirely new modifier of glucose homeostasis. When combined with our prior observations that CRP causes hypertension and impairs endothelial repair (13,14), these findings also indicate that CRP may be a common etiologic factor in the cardiovascular and metabolic disorders that often complicate chronic inflammatory conditions.

In the current study, CRP-induced insulin resistance was related to impaired skeletal muscle glucose delivery. This mechanism may also underlie the trend toward insulin resistance observed in TG-CRP mice fed normal chow in a recent report that did not interrogate how CRP affects insulin action (38). We reveal a mechanistic link between the attenuated skeletal muscle glucose delivery and the systemic insulin resistance caused by CRP because both were normalized in FcγRIIB$^{-/-}$ mice. Importantly, pancreatic insulin production, hepatic glucose production and insulin sensitivity, and adipose glucose uptake were unaffected by CRP. Consistent with these observations, we found that FcγRIIB is expressed in the skeletal muscle microvasculature but not in skeletal muscle myocytes, pancreatic islets, hepatocytes, or adipocytes. Also consistent with a key role for altered skeletal muscle vascular function and not altered myocyte function in CRP-induced insulin resistance, we found that CRP does not inhibit insulin-induced glucose uptake in isolated skeletal muscles studied ex vivo. Moreover, the primary defect of impaired skeletal muscle glucose delivery was fully prevented in the eNOS-S1176D mice expressing a phosphomimetic eNOS protected from CRP antagonism. From these multiple findings we conclude that CRP-induced insulin resistance is primarily due to impaired glucose delivery to skeletal muscle caused by FcγRIIB-mediated inhibition of endothelial insulin action.

Our current findings are consistent with the recognized interrelationship between NO, insulin action in endothelium, and metabolic homeostasis. The major aspects of the metabolic phenotype of the TG-CRP mice mirror observations in eNOS$^{-/-}$ mice. The latter have a decreased GIR during euglycemic-hyperinsulinemic clamping, blunted insulin-induced skeletal muscle blood flow, and skeletal muscle glucose delivery that is decreased by 40% compared with wild-type mice, whereas the response to insulin in ex vivo studies of skeletal muscle glucose uptake is normal (39). Furthermore, the attenuated skeletal muscle glucose uptake and consequences on global insulin sensitivity that we observe with CRP elevation are in close agreement with a recent report in which insulin receptor substrate 1 and 2 were both deleted from endothelium in a cell-specific manner (40). This phenocopying strengthens the evidence that the insulin resistance caused by CRP is most likely primarily due to adverse effects on insulin action in endothelium.

In addition to displaying insulin resistance, we discovered that older TG-CRP mice (13 weeks old) have increased fat mass. An increase in fat mass can contribute to the development of insulin resistance (41,42). However, this is not a primary mechanism in the current study because TG-CRP mice develop hyperglycemia and hyperinsulinemia as early as age 5 weeks, when fat mass is not increased, and the exogenous administration of recombinant CRP for 2 weeks causes hyperglycemia and hyperinsulinemia without affecting body composition. Mice with muscle-specific inactivation of the insulin receptor have increased fat mass (43), and the authors have speculated that this is due to the increase in glucose transport to adipose tissue also found in these mice (43). In TG-CRP mice, glucose uptake in adipose tissue is not altered. The basis for the increased adiposity found in older TG-CRP mice is yet to be elucidated.

clamp (insulin – or +) in 10–13-week-old WT or TG-CRP mice with insulin infusion at 4 mU/kg/min. Values are mean ± SEM, n = 14–15. *P < 0.05 vs. no insulin. In vivo glucose uptake was evaluated in WT or TG-CRP mice at age 10–13 weeks (*C* and *D*), or at age 5–6 weeks (*E* and *F*). Mice were injected intraperitoneally with [^{3}H]-2-DOG, and the specific accumulation of [^{3}H]-2-DOG-6-phosphate in white adipose tissue (WAT) isolated from the perigonadal fat pad (*C* and *E*) and soleus and gastrocnemius (Sol + Gas) skeletal muscle (*D* and *F*) was determined. Values are mean ± SEM, n = 5–6. *P < 0.05 vs. WT. *G*: Skeletal muscle blood flow was measured in 10–14-week-old WT or TG-CRP mice during a hyperinsulinemic-euglycemic clamp with insulin infusion at 20 mU/kg/min. Values are mean ± SEM, n = 6. *P < 0.05 vs 0 h, †P < 0.05 vs. WT at the indicated times. *H* and *I*: Effect of exogenous CRP on in vivo glucose uptake. WT mice were injected with vehicle or CRP 2 h before intraperitoneal injection of [^{3}H]-2-DOG, and the specific accumulation of [^{3}H]-2-DOG-6-phosphate in white adipose tissue (WAT) isolated from perigonadal fat pad (*H*) and soleus and gastrocnemius (Sol + Gas) skeletal muscle (*I*) was determined. Values are mean ± SEM, n = 6. *P < 0.05 vs. vehicle.

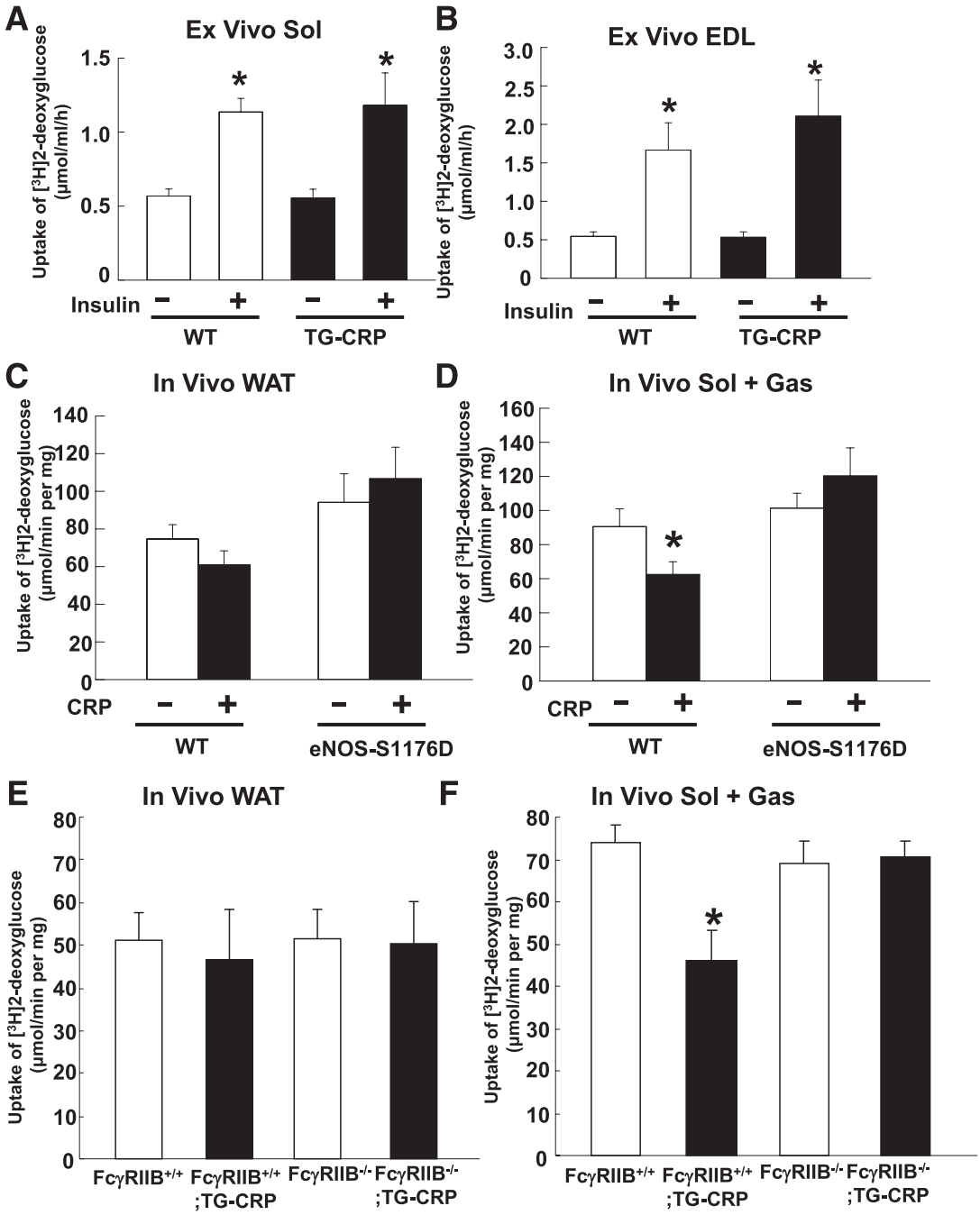

FIG. 6. FcγRIIB and eNOS antagonism mediate CRP impairment of skeletal muscle glucose delivery. *A* and *B*: Ex vivo glucose uptake was evaluated in isolated skeletal muscle in 10–13-week-old wild-type (WT) or TG-CRP mice. After muscles were harvested, basal and insulin-stimulated [^{3}H]-2-DOG uptake in soleus (Sol) (*A*) and extensor digitorum longus (EDL) (*B*) were measured ex vivo. Values are mean ± SEM, n = 3–5, *$P < 0.05$ vs. no insulin. *C* and *D*: Lack of CRP-induced inhibition of skeletal muscle glucose uptake in eNOS S1176D mice. Wild-type (WT) mice or eNOS-S1176D knock-in mice (10–13 weeks old) were injected with vehicle or CRP 2 h before an intraperitoneal injection of [^{3}H]-2-DOG, and the specific accumulation of [^{3}H]-2-DOG-6-phosphate in white adipose tissue (WAT) isolated from perigonadal fat pad (*C*) and soleus and gastrocnemius (Sol + Gas) skeletal muscle (*D*) was determined. Values are mean ± SEM, n = 9–11. *$P < 0.05$ vs vehicle. *E* and *F*: CRP impairment of in vivo skeletal muscle glucose uptake requires FcγRIIB. Male FcγRIIB$^{+/+}$, FcγRIIB$^{+/+}$;TG-CRP, FcγRIIB$^{-/-}$, and FcγRIIB$^{-/-}$;TG-CRP littermates (10–13 weeks old) were injected intraperitoneally with [^{3}H]-2-DOG, and the accumulation of [^{3}H]-2-DOG-6-phosphate in white adipose tissue (WAT) isolated from the perigonadal fat pad (*E*) and soleus and gastrocnemius (Sol + Gas) skeletal muscle (*F*) was determined. Values are mean ± SEM, n = 4–6. *$P < 0.05$ vs FcγRIIB$^{+/+}$.

Now knowing that CRP causes abnormal glucose homeostasis in mice and that FcγRIIB is critically involved, the role of CRP in insulin resistance in humans can be more effectively interrogated. Studies in lupus patients indicate that genetic variations in human FcγRIIB are common and that they impact receptor function (44), and there is also great variability in Fc receptor gene copy number (45). As such, there may be genetic modifiers of CRP action in humans, and previous studies that attempted to link CRP levels directly to phenotypes such as insulin resistance may have been oversimplified. Genetic variations in FcγRIIB can now be investigated to better understand how CRP contributes to the pathogenesis of insulin resistance in humans.

In summary, we have demonstrated that modest elevations in CRP cause insulin resistance in mice by decreasing skeletal muscle glucose delivery and that the process is due to attenuated endothelial insulin action mediated by FcγRIIB, which is abundant in skeletal muscle microvascular endothelium. By targeting the common underlying mechanism, namely endothelial dysfunction caused by the CRP-FcγRIIB tandem, future therapies aimed at CRP or its receptor may normalize the hypertension and insulin resistance that often accompany chronic inflammatory conditions.

ACKNOWLEDGMENTS

This work was supported by the American Diabetes Association Grant 1-10-BS-124 (C.M.), National Institutes of Health Grants HL-75473 (P.W.S.) and NS-33335 (P.L.H.), the Donald W. Reynolds Cardiovascular Clinical Research Center (W.V.), the O'Brien Kidney Center (W.V.), the American Heart Association Scientist Development Grant 0835344N (D.N.A.), and the Children's Medical Center of Dallas Research Foundation (P.W.S.).

P.W.S. reports having received honoraria for participation in scientific meetings at which data in this article were discussed. E.B. is an employee of MacroGenics, Inc., a company involved in the development of therapeutics antibodies and whose ch2.4G N297Q antibody was used in this study. No other potential conflicts of interest relevant to this article were reported.

K.T. and C.M. conceived the study, did experimental work, and wrote the manuscript. W.V. performed experimental work and assisted in data analysis and interpretation. J.A.B. performed quantitative RT-PCR analyses. D.N.A. and P.L.H. created the eNOS knock-in mice used in the study and assisted in data interpretation. E.B. contributed the monoclonal FcγRIIB antibodies, aided in the design of studies using the antibodies, and was involved in manuscript preparation. P.W.S. was involved in study conception, project planning, financing, supervision, data analysis, and manuscript preparation. C.M. and P.W.S. are the guarantors of this work and, as such, had full access to all the data in the study and take responsibility for the integrity of the data and the accuracy of the data analysis.

Parts of this study were presented at the Annual Scientific Sessions of the American Heart Association, Orlando, Florida, 14–18 November 2009.

The authors thank Christopher Longoria (University of Texas [UT] Southwestern Medical Center) and Mohamed Ahmed (UT Southwestern Medical Center) for technical assistance, Dr. Daniela Rogoff (UT Southwestern Medical Center) for her help in glucose uptake experiments, Dr. Jen-Chieh Chuang (UT Southwestern Medical Center) for pancreatic islet experiments, Dr. David Inuenza (MacroGenics, Inc) and Junko Umetani (UT Southwestern Medical Center) for immunohistochemical analysis, and Dr. Amira Klip (The Hospital for Sick Children, Toronto, Ontario, Canada) for providing them with L6-GLUT4myc cells. The authors also thank Drs. Philipp Scherer, Joyce Repa, Deborah Clegg, and Eric Berglund (all at UT Southwestern Medical Center) for their helpful discussion.

REFERENCES

1. Haffner SM. Insulin resistance, inflammation, and the prediabetic state. Am J Cardiol 2003;92:18J–26J
2. Festa A, D'Agostino R Jr, Howard G, Mykkänen L, Tracy RP, Haffner SM. Chronic subclinical inflammation as part of the insulin resistance syndrome: the Insulin Resistance Atherosclerosis Study (IRAS). Circulation 2000;102:42–47
3. Yudkin JS, Stehouwer CD, Emeis JJ, Coppack SW. C-reactive protein in healthy subjects: associations with obesity, insulin resistance, and endothelial dysfunction: a potential role for cytokines originating from adipose tissue? Arterioscler Thromb Vasc Biol 1999;19:972–978
4. Pradhan AD, Cook NR, Buring JE, Manson JE, Ridker PM. C-reactive protein is independently associated with fasting insulin in nondiabetic women. Arterioscler Thromb Vasc Biol 2003;23:650–655
5. Pradhan AD, Manson JE, Rifai N, Buring JE, Ridker PM. C-reactive protein, interleukin 6, and risk of developing type 2 diabetes mellitus. JAMA 2001; 286:327–334
6. Freeman DJ, Norrie J, Caslake MJ, et al.; West of Scotland Coronary Prevention Study. C-reactive protein is an independent predictor of risk for the development of diabetes in the West of Scotland Coronary Prevention Study. Diabetes 2002;51:1596–1600
7. Greenfield JR, Campbell LV. Relationship between inflammation, insulin resistance and type 2 diabetes: 'cause or effect'? Curr Diabetes Rev 2006;2: 195–211
8. Haffner SM. Abdominal adiposity and cardiometabolic risk: do we have all the answers? Am J Med 2007;120(Suppl. 1):S10–S16; discussion S16–S17
9. Haffner SM. The metabolic syndrome: inflammation, diabetes mellitus, and cardiovascular disease. Am J Cardiol 2006;97(2A):3A–11A
10. Kahn SE, Zinman B, Haffner SM, et al.; ADOPT Study Group. Obesity is a major determinant of the association of C-reactive protein levels and the metabolic syndrome in type 2 diabetes. Diabetes 2006;55:2357–2364
11. Lu J, Marnell LL, Marjon KD, Mold C, Du Clos TW, Sun PD. Structural recognition and functional activation of FcgammaR by innate pentraxins. Nature 2008;456:989–992
12. Marnell L, Mold C, Du Clos TW. C-reactive protein: ligands, receptors and role in inflammation. Clin Immunol 2005;117:104–111
13. Schwartz R, Osborne-Lawrence S, Hahner L, et al. C-reactive protein downregulates endothelial NO synthase and attenuates reendothelialization in vivo in mice. Circ Res 2007;100:1452–1459
14. Vongpatanasin W, Thomas GD, Schwartz R, et al. C-reactive protein causes downregulation of vascular angiotensin subtype 2 receptors and systolic hypertension in mice. Circulation 2007;115:1020–1028
15. Lin CS, Xia D, Yun JS, et al. Expression of rabbit C-reactive protein in transgenic mice. Immunol Cell Biol 1995;73:521–531
16. Xia D, Samols D. Transgenic mice expressing rabbit C-reactive protein are resistant to endotoxemia. Proc Natl Acad Sci USA 1997;94:2575–2580
17. Schleicher M, Yu J, Murata T, et al. The Akt1-eNOS axis illustrates the specificity of kinase-substrate relationships in vivo. Sci Signal 2009;2:ra41
18. Atochin DN, Wang A, Liu VW, et al. The phosphorylation state of eNOS modulates vascular reactivity and outcome of cerebral ischemia in vivo. J Clin Invest 2007;117:1961–1967
19. Sundgren NC, Zhu W, Yuhanna IS, et al. Coupling of Fcγ receptor I to Fcγ receptor IIB by Src kinase mediates C-reactive protein impairment of endothelial function. Circ Res 2011;109:1132–1140
20. Vicent D, Ilany J, Kondo T, et al. The role of endothelial insulin signaling in the regulation of vascular tone and insulin resistance. J Clin Invest 2003; 111:1373–1380
21. Cook S, Hugli O, Egli M, et al. Partial gene deletion of endothelial nitric oxide synthase predisposes to exaggerated high-fat diet-induced insulin resistance and arterial hypertension. Diabetes 2004;53:2067–2072
22. Zisman A, Peroni OD, Abel ED, et al. Targeted disruption of the glucose transporter 4 selectively in muscle causes insulin resistance and glucose intolerance. Nat Med 2000;6:924–928
23. Rogoff D, Ryder JW, Black K, et al. Abnormalities of glucose homeostasis and the hypothalamic-pituitary-adrenal axis in mice lacking hexose-6-phosphate dehydrogenase. Endocrinology 2007;148:5072–5080
24. Somwar R, Koterski S, Sweeney G, et al. A dominant-negative p38 MAPK mutant and novel selective inhibitors of p38 MAPK reduce insulin-stimulated glucose uptake in 3T3-L1 adipocytes without affecting GLUT4 translocation. J Biol Chem 2002;277:50386–50395
25. Hill JW, Elias CF, Fukuda M, et al. Direct insulin and leptin action on pro-opiomelanocortin neurons is required for normal glucose homeostasis and fertility. Cell Metab 2010;11:286–297
26. Ayala JE, Bracy DP, Julien BM, Rottman JN, Fueger PT, Wasserman DH. Chronic treatment with sildenafil improves energy balance and insulin action in high fat-fed conscious mice. Diabetes 2007;56:1025–1033
27. Steele R, Wall JS, De Bodo RC, Altszuler N. Measurement of size and turnover rate of body glucose pool by the isotope dilution method. Am J Physiol 1956;187:15–24
28. Chuang JC, Cha JY, Garmey JC, Mirmira RG, Repa JJ. Research resource: nuclear hormone receptor expression in the endocrine pancreas. Mol Endocrinol 2008;22:2353–2363

29. Ravetch JV, Bolland S. IgG Fc receptors. Annu Rev Immunol 2001;19:275–290
30. Vincent MA, Montagnani M, Quon MJ. Molecular and physiologic actions of insulin related to production of nitric oxide in vascular endothelium. Curr Diab Rep 2003;3:279–288
31. Zeng G, Nystrom FH, Ravichandran LV, et al. Roles for insulin receptor, PI3-kinase, and Akt in insulin-signaling pathways related to production of nitric oxide in human vascular endothelial cells. Circulation 2000;101:1539–1545
32. Steinberg HO, Brechtel G, Johnson A, Fineberg N, Baron AD. Insulin-mediated skeletal muscle vasodilation is nitric oxide dependent. A novel action of insulin to increase nitric oxide release. J Clin Invest 1994;94:1172–1179
33. Barrett EJ, Eggleston EM, Inyard AC, et al. The vascular actions of insulin control its delivery to muscle and regulate the rate-limiting step in skeletal muscle insulin action. Diabetologia 2009;52:752–764
34. Muniyappa R, Montagnani M, Koh KK, Quon MJ. Cardiovascular actions of insulin. Endocr Rev 2007;28:463–491
35. Richards OC, Raines SM, Attie AD. The role of blood vessels, endothelial cells, and vascular pericytes in insulin secretion and peripheral insulin action. Endocr Rev 2010;31:343–363
36. Mineo C, Gormley AK, Yuhanna IS, et al. FcgammaRIIB mediates C-reactive protein inhibition of endothelial NO synthase. Circ Res 2005;97:1124–1131
37. Tanigaki K, Mineo C, Yuhanna IS, et al. C-reactive protein inhibits insulin activation of endothelial nitric oxide synthase via the immunoreceptor tyrosine-based inhibition motif of FcgammaRIIB and SHIP-1. Circ Res 2009;104:1275–1282
38. Kaneko H, Anzai T, Nagai T, et al. Human C-reactive protein exacerbates metabolic disorders in association with adipose tissue remodelling. Cardiovasc Res 2011;91:546–555
39. Duplain H, Burcelin R, Sartori C, et al. Insulin resistance, hyperlipidemia, and hypertension in mice lacking endothelial nitric oxide synthase. Circulation 2001;104:342–345
40. Kubota T, Kubota N, Kumagai H, et al. Impaired insulin signaling in endothelial cells reduces insulin-induced glucose uptake by skeletal muscle. Cell Metab 2011;13:294–307
41. Rajala MW, Scherer PE. Minireview: the adipocyte—at the crossroads of energy homeostasis, inflammation, and atherosclerosis. Endocrinology 2003;144:3765–3773
42. Rutkowski JM, Davis KE, Scherer PE. Mechanisms of obesity and related pathologies: the macro- and microcirculation of adipose tissue. FEBS J 2009;276:5738–5746
43. Kim JK, Michael MD, Previs SF, et al. Redistribution of substrates to adipose tissue promotes obesity in mice with selective insulin resistance in muscle. J Clin Invest 2000;105:1791–1797
44. Smith KG, Clatworthy MR. FcgammaRIIB in autoimmunity and infection: evolutionary and therapeutic implications. Nat Rev Immunol 2010;10:328–343
45. Bournazos S, Woof JM, Hart SP, Dransfield I. Functional and clinical consequences of Fc receptor polymorphic and copy number variants. Clin Exp Immunol 2009;157:244–254